J. Fluid Mech. (2007), *vol.* 581, *pp.* 469–493.
doi:10.1017/S0022112007006040 Printed in the United Kingdom

Behaviour of a conducting drop in a highly viscous fluid subject to an electric field

N. DUBASH AND A. J. MESTEL

Department of Mathematics, Imperial College London, 180 Queen's Gate, London, SW7 2BZ, UK

(Received 18 August 2005 and in revised form 30 January 2007)

We consider the slow deformation of a relatively inviscid conducting drop surrounded by a viscous insulating fluid subject to a uniform electric field. The general behaviour is to deform and elongate in the direction of the field. Detailed numerical computations, based on a boundary integral formulation, are presented. For fields below a critical value, we obtain the evolution of the drop to an equilibrium shape; above the critical value, we calculate the drop evolution up to breakup. At breakup it appears that smaller droplets are emitted from the ends of the drop with a charge greater than the Rayleigh limit. As the electric field strength is increased the ejected droplet size decreases. A further increase in field strength results in the mode of breakup changing to a thin jet-like structure being ejected from the end. The shape of all drops is very close to spheroidal up to aspect ratios of about 5. Also, for fields just above the critical value there is a period of slow deformation which increases in duration as the critical field strength is approached from above. Slender-body theory is also used to model the drop behaviour. A similarity solution for the slender drop is obtained and a finite-time singularity is observed. In addition, the general solution for the slender-body equations is presented and the solution behaviour is examined. The slender-body results agree only qualitatively with the full numerical computations. Finally, a spheroidal model is briefly presented and compared with the other models.

1. Introduction

We examine the slow deformation of a conducting inviscid drop suspended in a viscous insulating fluid subject to a uniform electric field. The motivation for this work derives from the wide range of industrial settings where conducting drops are exposed to electric fields. Examples of these include electrohydrodynamic atomization, the purification of oils, the breakup of water drops in thunderstorms, and the behaviour of drops in ink-jet printers. An interesting and important application concerns the breakdown of dielectrics due to the presence of water droplets, cases of which occurred in the 1990s in pedestal insulators at UK power stations.

Pedestal insulators are large cylindrical ceramic insulators filled with bitumen, a very viscous insulating fluid. Between the ends of the insulators there is a high potential difference (about 300 kV phase to phase). Owing to faulty gaskets in the caps of the insulators, on a number of occasions rainwater leaked into the insulators and collected there. The accumulated water compromised the performance of the device, resulting in current spikes across the insulator, and in some cases catastrophic explosion. We use the pedestal insulator problem as the principal motivation of this work. However, rather than use the exact insulator geometry, we consider the more general problem of the deformation of a single inviscid conducting drop suspended in an infinite insulating viscous fluid subject to a uniform electric field.

Wilson & Taylor (1925) were the first to examine the shapes of bubbles in an electric field. In their experiments, they found some stable deformed shapes, as well as some bubbles with unstable pointed ends from which thin filaments were ejected. O'Konski & Thacher (1953) used a spheroidal approximation (where the drop is assumed to always be spheroidal in shape) along with an energy balance to determine the equilibrium spheroid for conducting and dielectric drops. It was found that below a critical electric field strength, conducting drops would attain an equilibrium. The spheroidal approximation has also been used by Abbi & Chandra (1956), Garton & Krasucki (1964), Taylor (1964), and Sherwood (1988) to study the equilibrium shapes for drops in a electric field. Additionally, Taylor (1964) calculated the angle for a pointed end on a conducting drop in equilibrium, and Ramos & Castellanos (1994) extended this work to dielectric drops. Higher modes of deformation were considered by Sample, Raghupathy & Hendricks (1970), and Grigor'ev, Sharov & Shiryaeva (1999) included effects of compressibility in the bubbles. Finally, Brazier-Smith (1971) and Miksis (1981) have calculated the equilibrium drop shapes numerically. The different approximations for the equilibrium shapes and for the critical electric field strength, while obtained from a variety of methods, are all in fairly good agreement. As the equilibrium shapes are independent of viscosity, all of these results are applicable to the case of a conducting drop suspended in a viscous fluid.

Slender-body theory has also been used to calculate the equilibrium shapes for conducting and dielectric drops (Sherwood 1991). Li, Halsey & Lobkovsky (1994) and Stone, Lister & Brenner (1999) determined the equilibrium shapes of conducting drops by matching the results of slender-body theory with Taylor's solution for conical ends. However, this work is more applicable to dielectric drops, where long and thin equilibrium drop shapes are possible, than to conducting drops where the 'longest' equilibrium shape has an aspect ratio of about 1.8.

Garton & Krasucki (1964) performed experiments with conducting drops suspended in another fluid. More recent experiments have been conducted by Ha & Yang (2000), Eow, Ghadiri & Sharif (2001), and Eow & Ghadiri (2003). The form of breakup (and the shape of the drop at breakup) is found to depend not only on the strength of the electric field, but also on the ratio of the viscosity of the drop to that of the surrounding fluid. Indeed, for the related problem of the deformation of bubbles and drops in slow extensional driving flows, Taylor (1934) showed that the viscosity ratio was critical in determining the mode of breakup of the drop. He found experimentally that when the surrounding fluid is much more viscous than the drop, it is possible to have a stable elongating drop that continues to elongate without any sign of breakup. However, for drops with a larger viscosity, droplets would break off from the ends. Hence we might expect the case of a conducting drop surrounded by a much more viscous fluid to behave differently from other viscosity combinations. Furthermore, in the limit of small drop viscosity, the behaviour should resemble that of the inviscid drop. Surprisingly, the case of an inviscid (or very low viscosity) drop has yet to be examined in depth.

The time-dependent deformation of drops has attracted little attention, and again, the case of a conducting drop surrounded by a much more viscous fluid has not been considered. In addition to calculating equilibrium drop shapes, Sherwood (1988) used boundary integral numerical computations to study the time-dependent behaviour of deforming drops. His results, however, were restricted to drops suspended in an equally viscous fluid. Other numerical work for dielectric drops has been done by Feng & Scott (1996), Baygents, Rivette & Stone (1998), and Hirata *et al.* (2000).

In this work we attempt to present a more complete picture of the behaviour of an inviscid drop suspended in a viscous fluid subject to an electric field. We

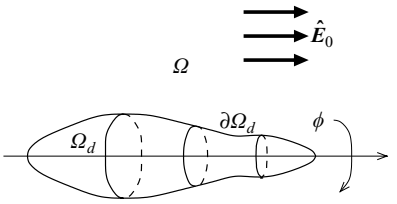

FIGURE 1. Physical setup of the problem.

begin in § 2 with a brief formulation of the problem. In § 3 numerical results based on boundary integral methods are presented. The behaviour of the drop right up to the point of breakup is determined. In addition, various characteristics of the breakup are examined. In § 4 we develop a slender-body model to study the dynamic behaviour of long and thin drops. For conditions where no equilibrium shape exists, it is reasonable to assume that the drop will elongate into a long slender drop and then either keep deforming indefinitely or undergo some form of breakup. We present a similarity solution, and examine the general time-dependent behaviour for slender drops. Finally, we end in § 5 with some concluding remarks. In the Appendix, we present a simplified spheroidal model that is compared to the other models. It is shown to be very accurate for deformations up to an aspect ratio of 5.

2. Problem formulation

We examine the slow deformation of a conducting fluid drop, surrounded by an insulating viscous fluid, subject to a uniform electric field, $\hat{\boldsymbol{E}}_0$. We assume that the problem is axisymmetric, with the axis of symmetry parallel to the electric field, and that the surrounding fluid is infinite in extent. The basic physical setup is shown in figure 1. We assume that the two fluids are immiscible, so that our domain is always divided into two simply connected regions: Ω_d, the fluid drop, and Ω, the surrounding fluid. The interface between the drop and the surrounding fluid is denoted by $\partial\Omega_d$. Both fluids are assumed to be incompressible and of equal density. We restrict our attention to the case where the surrounding fluid is highly viscous and the drop is relatively inviscid. Finally, we assume that far away from the drop the electric field is uniform and the fluid is stationary. Quantities denoted with a 'hat' are dimensional while quantities without a hat are dimensionless. We also adopt the Einstein summation convention for repeated indices.

Because we are considering slow deformation, we use the Stokes equations. For Stokes flow, time-dependence enters the problem only through the kinematic boundary condition for the drop surface. This implies that at each point in time we have an electrostatic problem for the electric field and a stationary Stokes problem (with an imposed surface stress) for the velocity field, that must be solved given the current drop shape; the drop shape then evolves via the kinematic condition.

2.1. *Physical equations and boundary conditions*

For a drop which is a good conductor, the time scale required for charge to move around on the surface of the drop is much smaller than the time scale on which the shape of the drop changes. Thus for the electric field we have an electrostatic problem: the electric field essentially adjusts instantaneously to any change in the drop shape. We can describe the electric field exterior to the drop, $\hat{\boldsymbol{E}}$, in terms of an

electric potential, $\hat{\theta}$,

$$\hat{\boldsymbol{E}} = -\hat{\nabla}\hat{\theta}. \tag{2.1}$$

The electric potential then satisfies Laplace's equation in the surrounding fluid:

$$\hat{\nabla}^2\hat{\theta} = 0 \quad \text{in } \Omega. \tag{2.2}$$

For a conducting drop the electric field at the surface of the drop must be normal to the surface. Hence the drop surface is a surface of constant electric potential; we can without loss of generality set that constant to zero:

$$\hat{\theta} = 0 \quad \text{on } \partial\Omega_d. \tag{2.3}$$

Finally, far away from the drop the electric field is uniform:

$$\hat{\nabla}\hat{\theta} \to -\hat{\boldsymbol{E}}_0 \quad \text{far away from the drop.} \tag{2.4}$$

Given the drop shape, (2.2)–(2.4) determine the electric potential, and thus the electric field surrounding the drop.

As we are only interested in the slow deformation (i.e. low-Reynolds-number regime) and the viscosity of the drop is insignificant compared to that of the surrounding fluid, we can assume that the unsteady and nonlinear inertial forces are negligible. Thus, the pressure inside the drop is spatially constant. (This constant does, however, change with time as the drop deforms.) Furthermore, we are not concerned with the flow inside the drop as the motion of the fluid in the drop has no effect on the surrounding flow; it merely moves as necessary to accommodate the deformation of the drop. Since the problem is axisymmetric, we can introduce the Stokes stream function, $\hat{\psi}$, for the flow in the surrounding fluid, the components of the velocity being expressible in terms of its derivatives. Then the stream function satisfies the equation

$$\hat{\mathrm{E}}^4\hat{\psi} = 0 \quad \text{in } \Omega. \tag{2.5}$$

A general expression for the operator $\hat{\mathrm{E}}^2$ in curvilinear coordinates can be found in Happel & Brenner (1965).

On the surface of the drop we must have a balance of stresses. As the drop is inviscid, the tangential stress on the surface must be zero:

$$\hat{\tau}_{ij}n_i t_j = 0 \quad \text{on } \partial\Omega_d, \tag{2.6}$$

where

$$\hat{\tau}_{ij} = \hat{\mu}\hat{\gamma}_{ij} = \hat{\mu}\left(\frac{\partial\hat{u}_i}{\partial\hat{x}_j} + \frac{\partial\hat{u}_j}{\partial\hat{x}_i}\right) \tag{2.7}$$

is the deviatoric stress tensor, $\boldsymbol{n}$ is the unit normal of the drop surface, $\boldsymbol{t}$ is a unit tangent vector of the drop surface, $\hat{\mu}$ is the viscosity of the surrounding fluid, and $\hat{\gamma}_{ij}$ is the rate-of-strain tensor. (Since our problem is axisymmetric, it is ϕ-independent, where ϕ is the azimuthal angle, and we only need to consider one tangent vector that lies in a plane $\phi =$ constant.) The normal stress on the surface must balance the internal drop pressure, the electric stress, and surface tension:

$$\hat{p}_d - \hat{p} + \hat{\tau}_{ij}n_i n_j + \frac{1}{2}\hat{\epsilon}_0\left(\frac{\partial\hat{\theta}}{\partial n}\right)^2 - \hat{\gamma}_s\hat{K} = 0 \quad \text{on } \partial\Omega_d, \tag{2.8}$$

where $\hat{p}_d$ is the internal drop pressure, $\hat{p}$ is the pressure in the surrounding fluid, $\hat{\epsilon}_0$ is the permittivity of the surrounding fluid, $\partial/\partial n$ is the normal derivative, $\hat{\gamma}_s$ is the surface tension, and $\hat{K}$ is twice the mean curvature of the drop surface. The electric

stress term in the normal stress balance is the only place where the electric field couples into the fluid flow. It is this term that drives the deformation of the drop.

Given the drop shape and the electric potential, (2.5), (2.6), and (2.8), combined with the condition of zero flow at infinity are sufficient to determine $\hat{\psi}$ (up to a constant), and hence the velocity, $\hat{\boldsymbol{u}}$, exterior to the drop. Finally, having determined $\hat{\boldsymbol{u}}$, the drop surface, $\partial\Omega_d$, which is denoted by a level set function $\hat{F}(\hat{\boldsymbol{x}}, \hat{t}) = 0$ for some function $\hat{F}$, evolves according to the kinematic condition

$$\frac{\partial \hat{F}}{\partial \hat{t}} + \hat{\boldsymbol{u}} \cdot \hat{\nabla} \hat{F} = 0. \tag{2.9}$$

Equations (2.2)–(2.6), (2.8), (2.9), plus conservation of mass for the drop (i.e. constant drop volume) and zero flow at infinity, form the full set of equations that govern the behaviour of the drop.

3. Boundary integral method

In this section we formulate the problem in terms of boundary integral equations. The resulting equations are then discretized for numerical computations. To non-dimensionalize the problem we construct the relevant length, time, and velocity scales from the physical parameters of the problem and make the following change to non-dimensional variables:

$$\hat{\nabla} = \frac{1}{\hat{L}}\nabla \qquad \hat{t} = \hat{T}t = \frac{\hat{\mu}\hat{L}}{\hat{\gamma}_s}t, \qquad \hat{u}_i = \hat{U}u_i = \frac{\hat{\gamma}_s}{\hat{\mu}}u_i, \qquad \hat{p} = \frac{\hat{\gamma}_s}{\hat{L}}p, \tag{3.1}$$

$$\hat{\dot{\gamma}}_{ij} = \frac{1}{\hat{T}}\dot{\gamma}_{ij} = \frac{\hat{\gamma}_s}{\hat{\mu}\hat{L}}\dot{\gamma}_{ij}, \qquad \hat{\theta} = \hat{E}_0\hat{L}\theta, \qquad \hat{\psi} = \hat{U}\hat{L}^2\psi = \frac{\hat{\gamma}_s\hat{L}^2}{\hat{\mu}}\psi, \tag{3.2}$$

where $\hat{L} = (3\hat{V}/(4\pi))^{1/3}$, $\hat{V}$ is the volume of the drop, and $\hat{E}_0 = |\hat{\boldsymbol{E}}_0|$.

With this scaling, viscosity $\hat{\mu}$ disappears from the problem, as it only affects the rate at which things happen. Only one parameter remains in the problem, the dimensionless electric field strength,

$$\beta = \frac{\hat{\epsilon}_0 \hat{E}_0{}^2 \hat{L}}{\hat{\gamma}_s}, \tag{3.3}$$

which appears in the non-dimensional version of (2.8):

$$p_d - p + \tau_{ij} n_i n_j + \frac{1}{2}\beta \left(\frac{\partial\theta}{\partial n}\right)^2 - K = 0 \quad \text{on } \partial\Omega_d. \tag{3.4}$$

3.1. *Boundary integral formulation*

Because of the electrostatic nature of the problem, the electric field can be calculated independently of the fluid flow. The electric stress, which is determined by the electric field, is then used in the calculation of the fluid flow.

Since the electric field potential satisfies Laplace's equation we can use precisely the same boundary integral formulation as Pozrikidis (1997, Ch. 10) for potential flow. For this formulation we require the electric potential to go to zero far away from the drop. Thus, we write

$$\theta(\boldsymbol{x}) = -x + \tilde{\theta}(\boldsymbol{x}). \tag{3.5}$$

Now $\tilde{\theta}(\boldsymbol{x}) = x$ on $\partial\Omega_d$ and $\tilde{\theta}(\boldsymbol{x}) \to 0$ far away from the drop. Then the boundary integral equation for the electric potential $\tilde{\theta}$ can be written

$$\tilde{\theta}(\boldsymbol{x}_0) = -2\int_{\partial\Omega_d} G(\boldsymbol{x}_0, \boldsymbol{x})\,\nabla\tilde{\theta}(\boldsymbol{x})\cdot\boldsymbol{n}(\boldsymbol{x})\,\mathrm{d}S(\boldsymbol{x}) + 2\int_{\partial\Omega_d}^{PV} \nabla G(\boldsymbol{x}_0, \boldsymbol{x})\cdot\boldsymbol{n}(\boldsymbol{x})\,\tilde{\theta}(\boldsymbol{x})\,\mathrm{d}S(\boldsymbol{x}) \quad (3.6)$$

where $G(\boldsymbol{x}_0, \boldsymbol{x}) = 1/(4\pi\rho)$ is the free-space Green's function of Laplace's equation, with $\rho = |\boldsymbol{x} - \boldsymbol{x}_0|$, $\boldsymbol{n}(\boldsymbol{x})$ is the outward normal of the drop surface (i.e. pointing into the surrounding fluid), ∇ is with respect to the point $\boldsymbol{x}$, and the superscript PV indicates the principal value of the integral (i.e. $\boldsymbol{x}_0$ lies on $\partial\Omega_d$). In equation (3.6), the integrals are respectively referred to as the single-layer potential and the double-layer potential.

With $\tilde{\theta}$ known on the drop surface, equation (3.6) becomes a Fredholm integral equation of the first kind which must be solved for $\nabla\tilde{\theta}\cdot\boldsymbol{n}$. To obtain $\nabla\theta\cdot\boldsymbol{n}$ we note that

$$\nabla\theta\cdot\boldsymbol{n} = -n_x + \nabla\tilde{\theta}\cdot\boldsymbol{n}. \quad (3.7)$$

The electric stress is then given by $\beta(\partial\theta/\partial\boldsymbol{n})^2/2 = \beta(\nabla\theta\cdot\boldsymbol{n})^2/2$.

Similarly we can write a boundary integral equation for the velocity field surrounding the drop. Following Pozrikidis (1992, Ch. 5), the integral equation for a relatively inviscid drop surrounded by a viscous fluid is

$$u_j(\boldsymbol{x}_0) = -\frac{1}{4\pi}\int_{\partial\Omega_d} \Delta f_i(\boldsymbol{x}) G_{ij}(\boldsymbol{x}_0, \boldsymbol{x})\,\mathrm{d}S(\boldsymbol{x}) + \frac{1}{4\pi}\int_{\partial\Omega_d}^{PV} u_i(\boldsymbol{x}) T_{ijk}(\boldsymbol{x}_0, \boldsymbol{x}) n_k(\boldsymbol{x})\,\mathrm{d}S(\boldsymbol{x}), \quad (3.8)$$

where G_{ij} is the Green's function of Stokes flow, T_{ijk} is the associated stress tensor, Δf_i is the jump in interfacial surface force across the drop surface, and n_i is the outward unit normal of the drop. Again we use the free-space Green's function and associated stress tensor, which are given by

$$G_{ij} = \frac{\delta_{ij}}{\rho} + \frac{\tilde{x}_i\tilde{x}_j}{\rho^3} \qquad \text{and} \qquad T_{ijk} = -6\frac{\tilde{x}_i\tilde{x}_j\tilde{x}_k}{\rho^5}, \quad (3.9)$$

where $\rho = |\tilde{\boldsymbol{x}}|$, $\tilde{\boldsymbol{x}} = \boldsymbol{x} - \boldsymbol{x}_0$, and δ_{ij} is the Kroneker delta.

The jump in interfacial surface force, Δf_i is given by

$$\Delta f_i = \left(\sigma_{ij}^{(1)} - \sigma_{ij}^{(2)}\right) n_j, \quad (3.10)$$

where σ_{ij} is the stress tensor, and the superscripts (1) and (2) denote the surrounding fluid and the fluid in the drop respectively. For the surrounding viscous fluid $\sigma_{ij}^{(1)} = -p\delta_{ij} + \dot{\gamma}_{ij}$, and for the inviscid drop $\sigma_{ij}^{(2)} = -p_d\delta_{ij}$. Thus (3.10) becomes

$$\Delta f_i = [(p_d - p)\delta_{ij} + \dot{\gamma}_{ij}]n_j = \left[K - \frac{1}{2}\beta\left(\frac{\partial\theta}{\partial n}\right)^2\right] n_i. \quad (3.11)$$

With Δf_i given, (3.8) becomes a set of Fredholm integral equations of the second kind for the velocity at the drop surface.

For axisymmetric flow the single-layer and double-layer integrals in (3.6) and (3.8) can be reduced to line integrals over a contour of the drop profile. We make a change of variables to cylindrical coordinates and perform the azimuthal integration analytically. The details of this are given in Pozrikidis (1997, 1992).

The details of the general numerical scheme are as follows. Given the drop shape, we solve the axisymmetric version of (3.6) and use (3.7) to obtain $\nabla\theta\cdot\boldsymbol{n}$. The jump in interfacial surface force, Δf_i, is then calculated from (3.11). The axisymmetric version

of (3.8) is solved for the fluid velocity at the surface of the drop. And finally, the drop interface is moved with the velocity of the fluid at the drop surface.

3.2. *Some specifics of the numerical implementation*

The drop profile is represented as a set of discrete marker points. The profile is assumed to be linear between any two marker points except at the very ends of the drop. For the endpoint intervals the profile, $x(r)$, is assumed to be quadratic in r such that the drop has a smooth rounded end. The curvature at a given marker point is calculated using finite differences. With the drop contour discretized, the boundary integral equations can be written as a set of discrete equations for the unknown functions evaluated at the marker points.

It should be noted that some of the kernels in the axisymmetric boundary integral equations have a singularity as $\boldsymbol{x} \to \boldsymbol{x}_0$. In an interval where an integrand becomes singular, the singular behaviour is subtracted from the integrand, integrated analytically, and then added back to the regular portion of the integral (which is calculated numerically). The boundary integral equations then result in a set of linear equations for the values of the unknown functions at the marker points. We use the 'dgesv' routine from the numerical package LAPACK to solve our systems of linear equations.

Also, the axisymmetric version of (3.8) turns out to have a infinite number of solutions for any function Δf_i (Pozrikidis 1992). Specifically we require the solution that conserves mass, i.e.

$$\int_{\partial\Omega_d} u_i(\boldsymbol{x}) n_i(\boldsymbol{x})\, \mathrm{d}S = 0. \tag{3.12}$$

A numerically calculated solution will, in general, not satisfy (3.12). To obtain the desired solution we also calculate the eigenfunction of the associated homogeneous equation and use a linear combination of the numerically calculated solution and the eigensolution which satisfies (3.12). Another way to obtain the desired solution is to regularize the boundary integral equation by removing the offending eigenvalue (see Pozrikidis 1992, Ch. 4). However, we found that our method, while more expensive computationally, conserves mass to a better degree.

Finally, once the fluid velocity at the marker points is calculated, we need to evolve the shape of the drop. We move the marker points with the normal velocity at the surface and add a tangential displacement to redistribute the marker points approximately evenly along the contour. Without this redistribution of marker points, regions of high distortion would become poorly resolved.

3.3. *Results*

For a variety of values of the dimensionless electric field strength, β, we begin with an initially spherical drop and then allow it to evolve.

If the strength of the electric field, represented by β in (3.4), is small enough, it is possible for equilibrium drop shapes to exist; the surface tension stress balances the electric stress. Above a critical electric field strength there are no equilibrium shapes and the drop will continue to deform until breakup. It was found that the critical electric field strength was between 0.204 and 0.2045 (which is in excellent agreement with the result of $\beta_{crit} \doteq 0.2044$ from the spheroidal approximation model (see the Appendix), and the results of other authors).

Figures 2 and 3 show drops at several times during their evolution. In figure 2, $\beta = 0.20$ and an equilibrium shape exists. In figure 3, $\beta = 0.30$ and no equilibrium shapes exist. The drop deforms until pinch-off occurs, at which point the numerical code stops. Initially the drop becomes dumbbell shaped ($t = 8$), but then proceeds

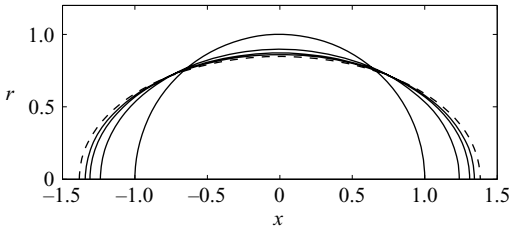

FIGURE 2. The shape of an initially spherical drop at times $t = 0, 4, 8, 12$ for $\beta = 0.20$, along with the equilibrium drop shape (dashed line).

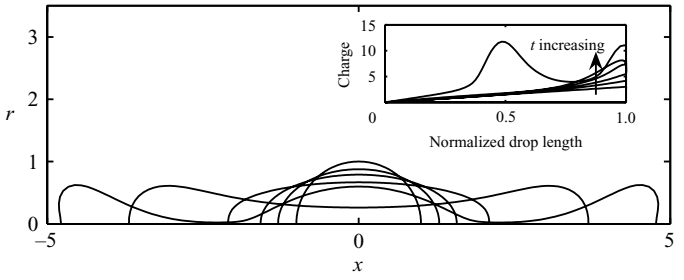

FIGURE 3. The shape of an initially spherical drop at times $t = 0, 2, 4, 6, 8, 9$ for $\beta = 0.30$. At time $t = 9.24$ the drop pinches off into three pieces. Shown in the inset is the charge along the drop surface for each time.

β	Volume as a fraction of the original drop	Magnitude of charge	Rayleigh limit	New β value for the remaining central drop
0.205	0.29	39	30	0.15
0.21	0.29	39	30	0.16
0.23	0.26	38	27	0.18
0.25	0.23	38	24	0.20
0.3	0.15	38	18	0.27
0.4	0.10	40	13	0.37
0.5	0.10	42	11	0.46

TABLE 1. Some characteristics of the lobes at the point of pinch-off for various values of β. The values given are for a single lobe.

to form a three-lobed shape. While the numerical solution stops at the point of pinch-off, we fully expect the lobes to detach and the drop to break apart into three. Furthermore, since charges tend to collect at sharp points, we expect there to be a significant amount of charge on the lobe at the point of pinch-off. The two droplets formed when the lobes detach will have charges that are equal in magnitude and opposite in sign and will move rapidly away from the remaining central drop. If the remaining central drop is below a critical size, it will relax to an equilibrium shape; if not, the process is likely to repeat.

Table 1 shows, for various values of β, some of the characteristics of the droplets formed when the lobes detach. The Rayleigh limit for the maximum charge that a spherical drop can have before becoming unstable is $\hat{Q}_c$, which is given by

$$\hat{Q}_c^2 = 64\pi^2 \hat{\epsilon}_0 \hat{\gamma}_s \hat{r}^3, \tag{3.13}$$

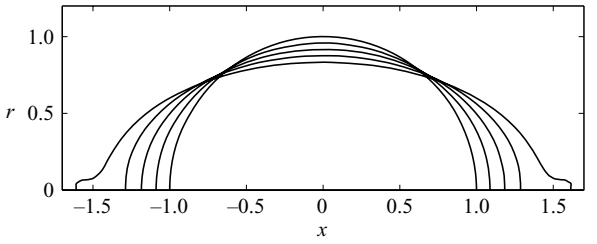

FIGURE 4. The shape of an initially spherical drop at times $t = 0, 0.2, 0.4, 0.6, 0.79$ for a strong electric field ($\beta = 0.70$).

where $\hat{r}$ is the radius of the spherical drop (Rayleigh 1882). Using our scalings, this can be written non-dimensionally as

$$Q_c^2 = \frac{64\pi^2 \tilde{V}}{\beta}, \tag{3.14}$$

where Q_c and $\tilde{V}$ are the dimensionless charge and volume as given in table 1. If we compare the critical charges with the numerically calculated values, we find that for all the drops the charges are above the Rayleigh limit. This indicates that the lobes, upon detaching from the central drop, would break apart further into smaller droplets. The fact that the droplets formed are highly charged appears to be a generic feature that is not directly dependent on the fluid properties or the magnitude of the electric field. Any droplet or jet that detaches from the main drop will have to do so by forming a region of very high (radial) curvature. Charge will accumulate there, resulting in a high concentration of charge on any portion of the drop that detaches. This general behaviour can be seen in figure 3 (inset).

It should be noted that the Rayleigh limit is for a charged drop in the absence of an electric field. For a charged drop accelerating in an electric field it is theoretically possible, in certain situations, to exceed the Rayleigh limit (Mestel 2002); however, the increase in the critical charge is by no more than a factor of two, which would still leave several of the droplets in table 1 supercritical. Also included in table 1 is the value of β for the remaining central drop. For higher initial β values, the remaining central drop is still supercritical and will probably undergo further breakup through the formation of another pair of lobes.

It can be seen from table 1 that as β increases the lobe volume decreases. At $\beta \gtrsim 0.6$ lobe formation disappears and the characteristics of breakup change. Instead of forming a dumbbell shape (see figure 3, $t = 8$), the drop always remains convex until a thin jet-like structure emerges from the endpoint (see figure 4). It should be noted that the velocities at the endpoint become very large and, in practice, inertia may become important. (Again, since charges accumulate at sharp points, there would be a large concentration of charge on the jet which would probably result in the jet breaking up into many smaller droplets.)

Ha & Yang (2000) performed some experiments where highly conducting drops suspended in another fluid deform and break apart in an electric field. In their examples where the surrounding fluid is much more viscous than the drop we can see this characteristic formation and detachment of lobes at the end of a drop, as well as the breakup into smaller drops. Eow & Ghadiri (2003) also show some drops where a lobe forms and detaches from the end of the drop. Moreover, they show one example where a lobe forms at one end of a drop, detaches, and then proceeds to

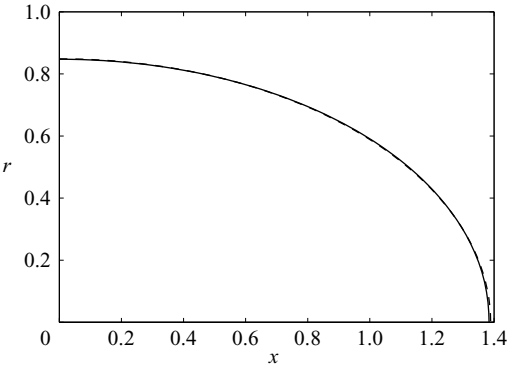

FIGURE 5. The numerically computed equilibrium drop shape (solid line) compared to that predicted by the spheroidal approximation model (dashed line) for $\beta = 0.20$.

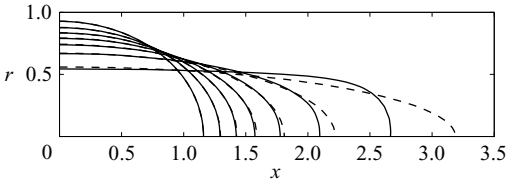

FIGURE 6. The numerically computed drop shapes from the boundary integral method (solid lines) compared to those predicted by the spheroidal approximation (dashed lines) for $\beta = 0.30$. The drop was initially spherical and the contours shown are for $t = 1, 2, 3, 4, 5, 6, 7$. For the first two times the two shapes fall directly on top of one another.

break apart into three smaller droplets. This is exactly the behaviour we expect if the droplet formed when the lobe detaches has a charge greater than the Rayleigh limit. Also, the phenomenon of a droplet cloud being ejected by a thin jet from the end of a drop has been seen by Garton & Krasucki (1964).

Results from Sherwood's (1988) boundary integral numerical simulations show that, for a conducting drop, pointed ends form just before the breakdown of his numerical scheme. We see no indication of pointed ends forming here. In Sherwood's work however, the viscosity of the drop and the surrounding fluid are equal, and it appears that the viscosity ratio of the drop to that of the surrounding fluid plays a significant role in the drop behaviour (Ha & Yang 2000; Dubash & Mestel 2007). This is certainly true for drops in deforming flows (Taylor 1934). However, in deforming flows low-viscosity drops form pointed ends and high-viscosity drops form lobes. It would appear that for drops in an electric field the opposite occurs; low-viscosity drops form lobes and high-viscosity drops form pointed ends.

For drops with an equilibrium shape, and even in the early stages for drops without an equilibrium shape, the shape of the deforming drop is very close to spheroidal. Figure 5 shows, for $\beta = 0.20$, the numerically computed equilibrium shape compared to the equilibrium shape predicted by the spheroidal approximation model of the Appendix. The difference is very small and is only noticeable near the end of the drop where the numerically computed shape is blunter than the spheroid. Indeed, only a small discrepancy was expected based on the results of Taylor (1964). Figure 6 compares the numerically computed shapes with the spheroidal shape predicted by the spheroidal approximation, for a drop with no equilibrium shape. The correspondence

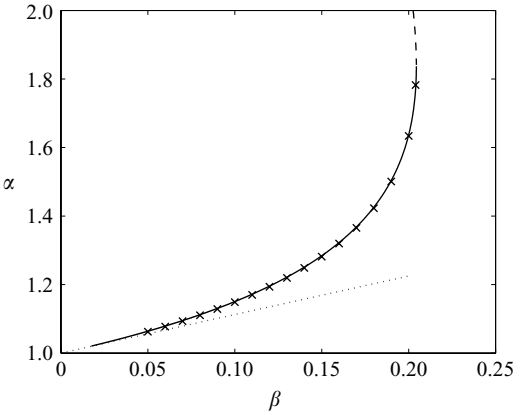

FIGURE 7. Equilibrium curve: the numerically computed equilibrium aspect ratios, α, for several values of β ($\times$). The solid line is the stable equilibrium curve calculated from the spheroidal approximation. The dashed portion of the line is the unstable equilibrium branch. The dotted line is the small-deformation result of Taylor (1966*b*).

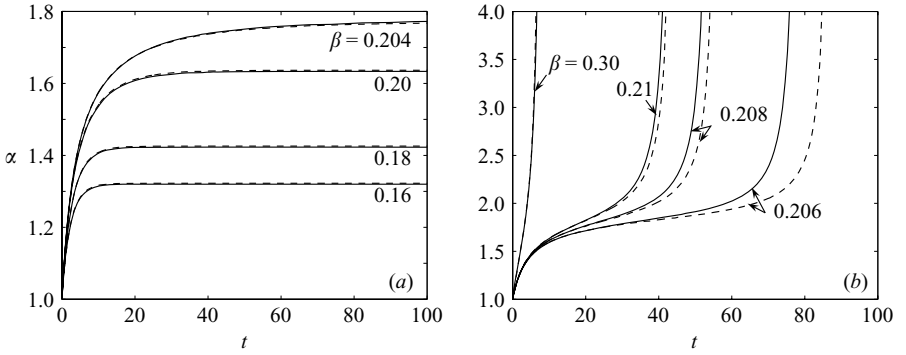

FIGURE 8. The evolution in time of drops: (*a*) drops for which there are equilibrium shapes, (*b*) drops for which there exist no equilibrium shapes. The numerical results are given by the solid lines. Also shown for comparison are the results for the spheroidal approximation (dashed line).

is quite good, except at large deformations, where the numerically calculated shape begins to deviate noticeable from a spheroid prior to the drop breaking up. For example, when $\beta = 0.3$, the spheroidal aspect ratio, α, is within 10 % of the exact result up to $\alpha = 4$.

Figure 7 shows the numerically computed equilibrium aspect ratios, α, for several values of β. For the numerical results we define the aspect ratio as the half-length of the drop divided by its radius at the point $x = 0$ (we use this definition of aspect ratio only while the drop is convex). Also shown is the equilibrium curve from the spheroidal approximation (see the Appendix). The difference is again quite small, with the numerically computed values being slightly lower than the spheroidal model for a given value of β.

Figure 8(*a*) shows a plot of the aspect ratio versus time for several values of β for which there exist equilibrium shapes. There is a good correspondence between the numerical results and the spheroidal model. The only discrepancy is again that

the numerical model predicts a slightly lower equilibrium aspect ratio (except for $\beta = 0.204$, which has yet to reach the equilibrium shape).

Figure 8(b) shows the evolution of drops for which $\beta > \beta_{crit}$, and no equilibrium shapes exist. Drops for which β is significantly larger than β_{crit} undergo rapid elongation (see figure 8b $\beta = 0.30$). However, where β is close to β_{crit} the drop experiences a period of slow elongation near the critical aspect ratio. As the critical electric field strength is approached from above, this period of slow elongation becomes longer and longer. Comparing the numerical results with the spheroidal approximation results in figure 8(b), the initial rates of deformation are well matched; however, the later time behaviour shows some discrepancies. It should be noted that the later time period of rapid deformation matches in both models, it is only in the period of slow deformation near the critical aspect ratio where the models differ.† The boundary integral numerical results show that this period of slow deformation is somewhat shorter than that predicted by the spheroidal model. And closer to the critical electric field strength the discrepancy becomes more pronounced. This is most likely due to a difference in the critical electric field strengths between the two models. If the critical value of β is lower in the boundary integral model, for a fixed value of $\beta > \beta_{crit}$ near the critical value, the distance from the critical value is larger for the numerical model. Therefore the numerical model is more likely to show a shorter period of slow deformation. Farther away from the critical electric field strength, where we no longer have this period of slow deformation, the discrepancy disappears; see figure 8(b), $\beta = 0.30$.

4. A model for slender drops

Here we consider drops that are long and slender, i.e. drops for which the radius from the axis of symmetry is much smaller than the drop length. Following Taylor (1966a) and Sherwood (1991) we model the electric field as a line distribution of point charges along the axis of the drop. The velocity field is modelled as the result of a line distribution of sources and sinks combined with a line distribution of point forces (Stokeslets). This idea has been successfully used by Buckmaster (1972, 1973) to model the equilibrium shapes, as well as the evolution of a slender drop in deforming external flows. It has also been used to model the equilibrium shapes of conducting and dielectric drops subject to an electric field (Sherwood 1991). We now use this idea to model the time-dependent deformation of a drop in an electric field.

4.1. *Governing equations in cylindrical coordinates*

Cylindrical coordinates, $(\hat{r}, \hat{x}, \phi)$, are used for the formulation. The drop shape is given by $\hat{r} = \hat{R}(\hat{x}, \hat{t})$ for $-\hat{\ell} \leqslant \hat{x} \leqslant \hat{\ell}$. Because of the physical symmetry of the problem we assume that the drop profile is symmetric about $x = 0$. The physical setup is illustrated in figure 9.

Given an initial drop shape, $\hat{R}(\hat{x}, 0)$, for $-\hat{\ell} \leqslant \hat{x} \leqslant \hat{\ell}$ (and recalling that $\hat{\ell} = \hat{\ell}(\hat{t})$), we scale lengths in the x-direction with $\hat{L} = \hat{\ell}(0)$ and lengths in the r-direction with $\hat{R}_0 = \hat{R}(0, 0)$. For a slender body we require

$$\epsilon = \frac{\hat{R}_0}{\hat{L}} \ll 1. \tag{4.1}$$

† Note that for all the numerical data shown in figure 8(b) the drop shape always remains convex. Once the drop profile becomes concave (e.g. figure 3, $t = 8$ or figure 4, $t = 0.79$) the aspect ratio is no longer a good measurement of the drop shape.

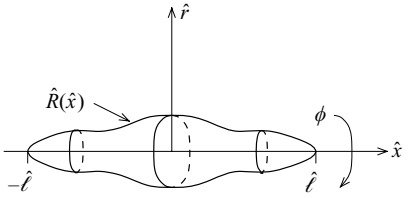

FIGURE 9. Physical setup in cylindrical coordinates.

Instead of (3.1) and (3.2) we use the following scalings for our slender-body analysis:

$$\hat{x} = \hat{L}x, \qquad \hat{r} = \hat{R}_0 r, \qquad \hat{t} = \frac{\epsilon \hat{L}}{\hat{U}}t, \qquad \hat{u}_r = \frac{\hat{U}}{\epsilon}u_r, \qquad \hat{u}_x = \frac{\hat{U}}{\epsilon^2}u_x, \tag{4.2}$$

$$\hat{p} = \frac{\hat{\mu}\hat{U}}{\epsilon^2 \hat{L}}p, \qquad \hat{\tau}_{ij} = \frac{\hat{\mu}\hat{U}}{\epsilon^2 \hat{L}}\tau_{ij}, \qquad \hat{\theta} = \delta \hat{E}_0 \hat{L}\theta, \qquad \hat{\psi} = \hat{U}\hat{L}^2\psi, \tag{4.3}$$

where $\hat{U} = \hat{\gamma}_s/\hat{\mu}$ is the velocity scale used previously. The factor of δ is included in the scaling of $\hat{\theta}$ because, physically, it is the electric stress on the surface of the drop that causes the deformation and drives the fluid motion. Thus, we will require the electric stress to balance with the viscous stresses at lowest order. Later on we will fix $\delta = \ln(1/\epsilon)$ to ensure that this occurs.

If $C(x)$ is a line distribution of point charges located on the axis of the drop with $-\ell \leqslant x \leqslant \ell$, then the electric potential resulting from the distribution and the uniform field is given by (Taylor 1966*a*)

$$\theta(r, x) = -x + \int_{-\ell}^{\ell} \frac{C(s)}{[(x-s)^2 + \epsilon^2 r^2]^{1/2}}\,\mathrm{d}s. \tag{4.4}$$

For a line distribution of sources/sinks, $q(x)$, and a line distribution of point forces, $\sigma(x)$, located on the axis of the drop with $-\ell \leqslant x \leqslant \ell$, the stream function is given by

$$\psi = -\int_{-\ell}^{\ell} \frac{q(s)(x-s)}{[(x-s)^2 + \epsilon^2 r^2]^{1/2}}\,\mathrm{d}s + \epsilon^2 r^2 \int_{-\ell}^{\ell} \frac{\sigma(s)}{[(x-s)^2 + \epsilon^2 r^2]^{1/2}}\,\mathrm{d}s. \tag{4.5}$$

Positive q represents a source and negative q is a sink, while positive σ represents a point force in the positive x-direction.† (Even though the second integral in (4.5) has a factor of ϵ^2 in front of it, because of the close-to-singular nature of the actual integral, the contribution from the σ term will still be significant at first order. However, it will be found that σ takes a passive role.) For conservation of mass we also require

$$\int_{-\ell}^{\ell} q(s)\,\mathrm{d}s = 0. \tag{4.6}$$

Finally, the pressure associated with ψ is

$$p = 2\epsilon^2 \int_{-\ell}^{\ell} \frac{\sigma(s)(x-s)}{[(x-s)^2 + \epsilon^2 r^2]^{3/2}}\,\mathrm{d}s. \tag{4.7}$$

† To return to dimensional variables $\hat{C}(\hat{x}) = 4\pi\hat{\epsilon}_0\hat{E}_0\hat{L}C(x)$, $\hat{q}(\hat{x}) = 4\pi\hat{U}\hat{L}q(x)$, and $\hat{\sigma}(\hat{x}) = 8\pi\hat{\mu}\hat{U}\sigma(x)$.

Note that because of symmetry about the plane $x = 0$, the stream function must be an odd function of x. This requires $q(x)$ to be an even function and $\sigma(x)$ to be an odd function.

The electric potential, (4.4), already satisfies Laplace's equation and the condition at infinity, (2.4). We need only consider the boundary condition on the surface of the drop, which is now

$$\theta = 0 \qquad \text{on } r = R(x). \tag{4.8}$$

The stream function, (4.5), already satisfies (2.5) and the condition of zero flow at infinity. So we need only consider the boundary conditions on the surface of the drop. With the scalings (4.2) and (4.3) the boundary conditions, (2.6), (2.8), and (2.9) can now be written

$$\tau_{nt} = 0 \qquad \text{on } r = R(x), \tag{4.9}$$

$$p_d - p + \tau_{nn} + \frac{1}{2}\delta^2\beta\left(\frac{\partial\theta}{\partial n}\right)^2 - \epsilon K = 0 \qquad \text{on } r = R(x), \tag{4.10}$$

$$-\frac{\partial R}{\partial t} + u_r - R'u_x = 0 \qquad \text{on } r = R(x), \tag{4.11}$$

respectively, where the prime denotes differentiation with respect to x and β is the dimensionless electric field strength given by (3.3).

4.2. *Electric stress*

Imposing (4.8) on the electric potential, we obtain

$$-x + \int_{-\ell}^{\ell} \frac{C(s)}{[(x-s)^2 + \epsilon^2 R^2]^{1/2}}\,\mathrm{d}s = 0. \tag{4.12}$$

Following the method of Tillett (1970) we can asymptotically approximate the integral in (4.12) for small ϵ. To leading order in ϵ we obtain

$$C(x) = \frac{1}{2}x\left[\ln\left(\frac{2\sqrt{\ell^2 - x^2}}{\epsilon R}\right)\right]^{-1}. \tag{4.13}$$

Using (4.4), and asymptotic approximations for the integrals, we obtain

$$\frac{\partial\theta}{\partial r} \approx -\frac{x}{r}\left[\ln\left(\frac{1}{\epsilon}\right)\right]^{-1} \qquad \text{and} \qquad \frac{\partial\theta}{\partial x} \approx -\left[\ln\left(\frac{1}{\epsilon}\right)\right]^{-1}. \tag{4.14}$$

Approximations (4.14) are valid everywhere except in a small region near $x = \pm\ell$ or when $R(x)$ is of size $O(\epsilon)$.

The normal and tangent vectors to the surface are given by

$$\boldsymbol{n} = (n_r, n_x) = [1 + \epsilon^2(R')^2]^{-1/2}(1, -\epsilon R'), \qquad \boldsymbol{t} = (t_r, t_x) = [1 + \epsilon^2(R')^2]^{-1/2}(\epsilon R', 1). \tag{4.15}$$

Thus, away from the endpoints of the drop, the electric stress is

$$\frac{1}{2}\left(\frac{\partial\theta}{\partial n}\right)^2 \approx \frac{1}{2}\frac{x^2}{\epsilon^2 r^2}\left[\ln\left(\frac{1}{\epsilon}\right)\right]^{-2} \qquad \text{on } r = R(x). \tag{4.16}$$

4.3. *Fluid motion*

To determine the stream function we need to calculate the source/sink distribution and the point force distribution from the boundary conditions on the drop surface.

Equations (4.9) and (4.10), when written in terms of the stream function, give two integral equations relating the unknown distributions, $q(x)$ and $\sigma(x)$. Using asymptotic approximations for small ϵ, these can be reduced to a system of differential equations which we are then able to solve for $q(x)$ and $\sigma(x)$. Once $q(x)$ and $\sigma(x)$ are known, equation (4.11) tells us how the drop shape evolves in time.

We substitute (4.15) and (4.16) into (4.9)–(4.11), write the components of velocity and stress in terms of the stream function (4.5), and then using asymptotic approximations for the integrals (Tillett 1970), we obtain (to first order)

$$q' - \sigma - \frac{R'q}{R} = 0, \tag{4.17}$$

$$2p_d R^2 - 8q + \beta x^2 = 0, \tag{4.18}$$

$$\frac{\partial R}{\partial t} - \frac{2q}{R} = 0. \tag{4.19}$$

We have set $\delta(\epsilon) = \ln(1/\epsilon)$ so that the electric stress term balances with the pressures and the viscous stress, and have assumed that $\beta = O(1)$. It turns out that surface tension is negligible at highest order. If we consider the normal stress balance, (2.8), away from the ends of the drop, the surface tension stress is $O(1/\epsilon)$; however the viscous stresses are $O(1/\epsilon^2)$. This is also observed in the spheroidal model (presented in the Appendix), where for high-aspect-ratio drops the change in surface tension energy was several orders of magnitude smaller than the viscous dissipation.

Equations (4.18) and (4.19) plus conservation of mass, (4.6), govern the deformation of the drop in our slender-body theory approximation. The value of σ is then determined *a posteriori* from (4.17). The system is valid away from the endpoints of the drop, where $R' \sim O(1)$; where R' is large the approximations made are no longer valid.

For our future analysis we rewrite (4.17)–(4.19) in a slightly more convenient form. From (4.18) we can solve for q. Substituting for q and q' in (4.19) and (4.17) we obtain a single equation for the evolution of the drop shape in terms of $R(x)$ and p_d, and equations for $\sigma(x)$ and $q(x)$ in terms of $R(x)$ and p_d:

$$\frac{\partial R}{\partial t} = \tfrac{1}{4}\beta\frac{x^2}{R} + \tfrac{1}{2}p_d R, \tag{4.20}$$

$$\sigma = \tfrac{1}{4}\beta x + \tfrac{1}{4}p_d R R' - \tfrac{1}{8}\beta\frac{R'x^2}{R}, \tag{4.21}$$

$$q = \tfrac{1}{8}\beta x^2 + \tfrac{1}{4}p_d R^2. \tag{4.22}$$

4.4. *Results for slender drops*

4.4.1. *Similarity solution*

For the set of equations (4.20)–(4.22) we look for a similarity solution. It turns out that for the slender-body model a finite-time singularity can be shown to exist. Hence we, *a priori*, modify the method slightly to incorporate this singularity.

Using (4.22) and symmetry in the plane $x = 0$, (4.6) is equivalent to

$$\int_0^{\ell(t)} (\beta x^2 + 2p_d R^2)\,\mathrm{d}x = 0 \Rightarrow \frac{1}{3}\beta\ell^3 + \frac{V}{\pi}p_d = 0,$$

$$\Rightarrow p_d = -\frac{\pi\beta\ell^3}{3V}, \tag{4.23}$$

where $V = 2\int_0^{\ell(t)} \pi R^2 \, \mathrm{d}x$ is the (non-dimensional) volume of the drop. Hence we can write (4.20) as

$$R\frac{\partial R}{\partial t} = \frac{1}{4}\beta x^2 - \frac{\pi\beta}{6V}\ell^3 R^2. \tag{4.24}$$

In equation (4.24) we make the following substitutions

$$x = \xi(t_c - t)^{\alpha}, \qquad R(x) = \rho(\xi)(t_c - t)^{\gamma}, \tag{4.25}$$

where ξ and $\rho(\xi)$ are the similarity variables, t_c is the unknown critical time where the finite-time singularity occurs, and α and γ are unknown exponents. From (4.25) it follows that the endpoint of the drop is given by

$$\ell(t) = \lambda(t_c - t)^{\alpha}, \tag{4.26}$$

where λ is a constant. In terms of the similarity variables, (4.24) becomes

$$-(\xi\rho^2)' = \frac{3}{2}\beta\xi^2 - \frac{\pi\beta}{V}\lambda^3\rho^2, \tag{4.27}$$

where the prime now denotes differentiation with respect to ξ, and we have chosen

$$\alpha = -\tfrac{1}{3}, \qquad \gamma = \tfrac{1}{6} \tag{4.28}$$

to eliminate time from the problem.

Solving (4.27), and applying the boundary condition $\rho = 0$ at $\xi = \lambda$ we obtain

$$\rho^2 = \begin{cases} \dfrac{3\beta}{2(3 - \pi\beta\lambda^3/V)}\left(\lambda^{(3-\pi\beta\lambda^3/V)}\xi^{(\pi\beta\lambda^3/V-1)} - \beta\xi^2\right) & \text{if } \dfrac{\pi\beta}{V}\lambda^3 \neq 3 \\ \tfrac{3}{2}\beta\xi^2 \ln(\lambda/\xi) & \text{if } \dfrac{\pi\beta}{V}\lambda^3 = 3. \end{cases} \tag{4.29}$$

The only value of the parameter $\pi\beta\lambda^3/V$ for which a 'drop-like' solution is obtained, is for

$$\frac{\pi\beta}{V}\lambda^3 = 1. \tag{4.30}$$

For all other values of this parameter either $\rho \to 0$, or $\rho \to \infty$ as $\xi \to 0$. With $\pi\beta\lambda^3/V = 1$, (4.29) reduces to

$$\rho^2 = \tfrac{3}{4}\beta(\lambda^2 - \xi^2). \tag{4.31}$$

The point source/sink distribution and the point force distribution can then be written

$$q = \beta Q(\xi)(t_c - t)^{-2/3}, \qquad \sigma = \beta\Sigma(\xi)(t_c - t)^{-1/3}, \tag{4.32}$$

where the similarity variables $Q(\xi)$ and $\Sigma(\xi)$ are given by

$$Q(\xi) = \frac{3}{16}\xi^2 - \frac{1}{16}\lambda^2, \qquad \Sigma(\xi) = \frac{5}{16}\xi + \frac{\xi^3}{8(\lambda^2 - \xi^2)}. \tag{4.33}$$

It can be seen that, as expected, ρ and Q are even functions, while Σ is an odd function.

4.4.2. *Initial value problem*

In addition to the similarity solution we can consider the initial value problem for a slender drop. Given an initial drop shape, (4.24) determines how it deforms and evolves in time.

In order to avoid singularities at the endpoint of the drop due to a rounded end it is more convenient to perform calculations using the variable

$$W(x,t) = R^2(x,t) \tag{4.34}$$

for the drop shape instead of $R(x,t)$. Also, by scaling t, x, and R we can eliminate β and π/V from (4.24). Thus we can, without loss of generality, write

$$\frac{\partial W}{\partial t} = \tfrac{1}{2}x^2 - \tfrac{1}{3}\ell^3 W. \tag{4.35}$$

Also, equation (4.11) evaluated at $\ell(t)$ gives an equation for the evolution of $\ell(t)$:

$$\frac{\mathrm{d}\ell}{\mathrm{d}t} = -\frac{\partial W}{\partial t}\bigg|_{x=\ell} \Big/ \frac{\partial W}{\partial x}\bigg|_{x=\ell}. \tag{4.36}$$

Given an initial drop shape $W(x,0) = \tilde{W}_0(x)$, $|x| \leqslant \ell(0)$ we look for a solution $W(x,t)$ and $\ell(t)$, with $W(\ell,t) = 0$, that satisfies (4.35). If we define the integrating factor

$$h(t) = \exp\left(\int_0^t \tfrac{1}{3}\ell^3(s)\,\mathrm{d}s\right), \tag{4.37}$$

then the general solution of (4.35) can be written

$$W(x,t) = \frac{1}{h(t)}\left(\tfrac{1}{2}x^2\int_0^t h(s)\,\mathrm{d}s + W_0(x)\right) \qquad \text{for} \quad |x| \leqslant \ell(t) \tag{4.38}$$

(and $W = 0$ for $|x| > \ell(t)$), where $W_0(x)$ is the analytic continuation of $\tilde{W}_0(x)$ from its original domain. To satisfy $W(\ell,t) = 0$ we require

$$W_0(\ell) = -\tfrac{1}{2}\ell^2\int_0^{t(\ell)} h(s)\,\mathrm{d}s \qquad \text{for} \quad \ell > \ell(0). \tag{4.39}$$

It can be verified that (4.38) conserves mass.

Differentiating (4.39) twice and after some manipulation we can obtain

$$f''(\ell)\left(\frac{\mathrm{d}\ell}{\mathrm{d}t}\right)^2 + f'(\ell)\frac{\mathrm{d}^2\ell}{\mathrm{d}t^2} = \frac{1}{3}\ell^3 f'(\ell)\frac{\mathrm{d}\ell}{\mathrm{d}t}, \tag{4.40}$$

where

$$f(x) = \left(\frac{W_0(x)}{x^2}\right). \tag{4.41}$$

This differential equation can be solved to obtain

$$t = \int_{\ell(0)}^{\ell} \frac{f'(x)}{\displaystyle\int_{\ell(0)}^{x} \tfrac{1}{3}s^3 f'(s)\,\mathrm{d}s - \tfrac{1}{2}}\,\mathrm{d}x. \tag{4.42}$$

Given an initial condition, (4.42) determines $t(\ell)$, and inverting this we can obtain $W(x,t)$ from (4.38). However, the integrals involved can only be solved analytically for suitably simple initial drop profiles, $W_0(x)$.

We can also compute the solution numerically directly from (4.35). Figure 10 shows the evolution in time for an initially spheroidal drop. Beginning with a spheroidal initial condition we are able to obtain the similarity solution, which in this case is

$$R^2 = \tfrac{3}{4}\left[(1-t)^{1/3} - (1-t)x^2\right]. \tag{4.43}$$

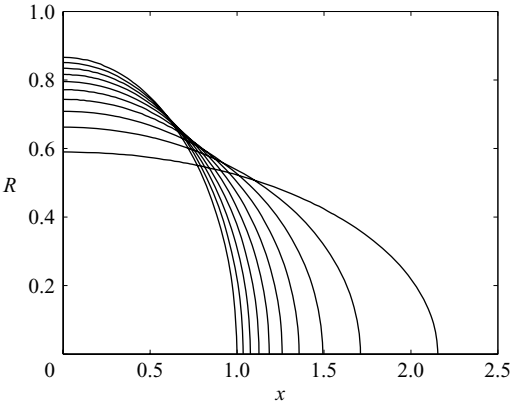

FIGURE 10. Evolution of a slender drop in time. The initial drop profile is $R^2 = 3(1 - x^2)/4$. The drop shape is given for $t = 0$ to $t = 0.9$ with $\Delta t = 0.1$; $t_c = 1.0003$. Note that the axes are given in terms of the scaled variables, whereas the physical width is $\epsilon \hat{R}$.

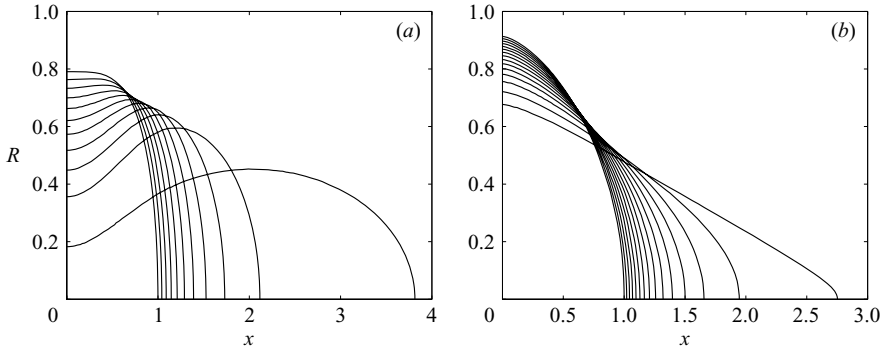

FIGURE 11. Time evolution of slender drops. (*a*) The initial drop profile is $R^2 = 5(1 - x^4)/8$. The drop shape is given for $t = 0$ to $t = 2.0$ with $\Delta t = 0.2$; $t_c = 2.04$. (*b*) The initial drop profile is $R^2 = 5(1 - x^{3/2})/6$. The drop shape is given for $t = 0$ to $t = 0.65$ with $\Delta t = 0.05$, and $t = 0.685$; $t_c = 0.686$.

It can be seen in figure 10 that the drop shape is always spheroidal. Also, for the numerical results of figure 10 we obtain $t_c = 1.0003$, which is in excellent agreement with $t_c = 1$ from (4.43). (In terms of the numerical computations, t_c corresponds to the point in time when one of the quantities involved goes to infinity.)

Figure 11 shows the evolution of drops whose initial profiles are not spheroidal. Figure 11(*a*) shows a drop whose end is blunter than a spheroid. In this case the drop appears to pinch-off into two lobes. Figure 11(*b*) shows a drop whose end is sharper than a spheroid. Here the drop profile becomes more pointed as it evolves. These two types of final shapes, two lobes or pointed ends, appear to be characteristic of the slender-body theory equations; all drops appear to evolve to one of these final shapes (except the similarity solution).

The long-term behaviour of the slender-body model is controlled by $f(x)$, and in particular by the sign of $f'(x)$. Slight changes in the analytical form of the initial shape $W_0(x)$ can lead to very different long-time behaviour. If $f(x)$ is strictly decreasing for

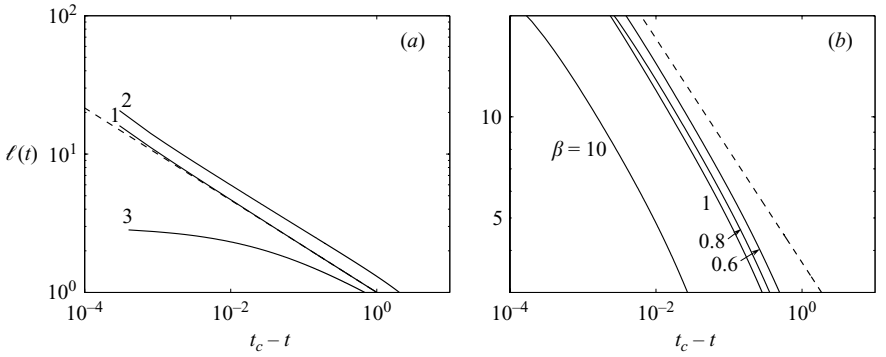

FIGURE 12. (*a*) Evolution of $\ell(t)$ for the numerical computations of the slender-body equations (solid lines). Curves 1, 2, and 3 correspond to the drops in figures 10, 11(*a*), and 11(*b*) respectively. (*b*) Evolution of $\ell(t)$ from the spheroidal approximation (solid lines). The slope predicted by the similarity solution is given by the dashed line.

$x > \ell(0)$ then, as $\ell \to \infty$,

$$t \to t_c = \int_{\ell(0)}^{\infty} \frac{3f'(x)}{\int_{\ell(0)}^{x} s^3 f'(s)\,\mathrm{d}s - \frac{1}{2}}\,\mathrm{d}x, \tag{4.44}$$

and the drop may blow up in a finite time. Combining (4.42) and (4.44), it can be seen that if $f'(x) \propto x^n$ as $x \to \infty$, for some $n > -4$, then $\ell \sim (n+4)^{1/3}(t_c - t)^{-1/3}$ and $W \propto (t_c - t)^{1/3}$. An example with $n = 1$ is given in figure 11(*a*). If on the other hand $f'(x) \propto \mathrm{e}^x$ as $x \to \infty$ then $\ell \sim [3(t_c - t)/2]^{-1/2}$. Moreover if $f'(x) \propto \mathrm{e}^{x^4}$, then the integral in (4.44) does not converge and $t_c \to \infty$.

However, if $f'(\ell_c) = 0$ for some $\ell_c > \ell(0)$, then the drop elongates in a finite time until $\ell = \ell_c$, at which point $\mathrm{d}\ell/\mathrm{d}t$ becomes infinite. It follows from (4.36) that $W_x(\ell_c) = 0$ and hence locally $W \propto (\ell_c - x)^2$, so that the drop develops a pointed end. This behaviour is shown in figure 11(*b*). The derivation of the slender-body equations breaks down at this point, as both the electric and capillary stresses become infinite. Furthermore, a direct balance between the two would require the cone to adopt the Taylor angle in violation of the slender-body assumption.

If an initially convex drop shape satisfies $f'(x) < 0$ for $x > 0$, it may remain convex or it may develop a dumbbell shape. However, differentiating (4.35) twice with respect to x, it becomes clear that if the curvature W_{xx} becomes positive, it remains so for all time (as can be seen in figure 11*a*). The time behaviour of $\ell(t)$ is shown in figure 12. Naturally, the development of a pointed end does not follow the $(t_c - t)^{-1/3}$ behaviour.

Since the detailed drop behaviour depends on the analytic continuation of $W_0(x)$ for $x > 1$, it is no surprise that the problem is numerically ill-conditioned. Except for the quadratic initial condition of the similarity solution, there is a reasonable variation between the predicted numerical and analytic blow-up times.

In addition, it appears that the similarity solution is unstable. Any small errors in the numerical computations result in the drop shape evolving from spheroidal to a shape similar to one of those in figure 11. Only if the approximations made in the numerical computations are exact for quadratic polynomials can we obtain the similarity solution. Physically, we expect the spheroidal shape to become unstable if the drop is to break up.

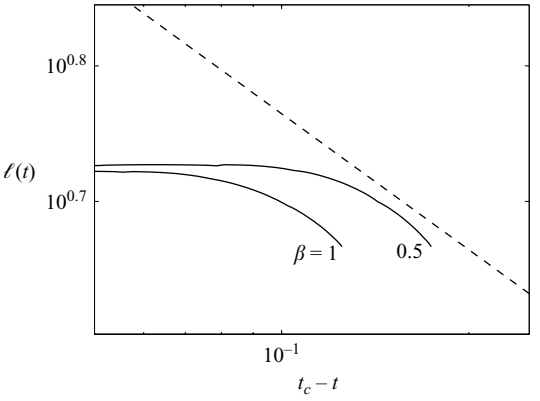

FIGURE 13. Evolution of $\ell(t)$ for long and slender drops from the boundary integral calculations (solid lines). The initial drop shape was a spheroid of aspect ratio 10. The dashed line indicates the slope of the slender-body similarity solution.

We can also examine the behaviour of $\ell(t)$ from the spheroidal approximation of the Appendix; see figure 12(*b*). For later time, as $t \to t_c$ even the spheroidal approximation model exhibits a $(t_c - t)^{-1/3}$ behaviour.

Unfortunately, the boundary integral results do not compare well with the slender-body calculations. Even if we begin the boundary integral calculations with a spheroidal drop with a high aspect ratio (and $\beta > \beta_{crit}$), we find that there is a very brief period of elongation, but then small lobes form at the ends of the drop and breakup occurs. The similarity solution (4.31) is not seen, nor are the time-dependent shapes given in figure 11. The brief period of elongation does, however, approximately match the scalings of the similarity solution (see figure 13), though, when the lobes begin to form the drop length no longer increases, and this correspondence is lost. It is likely that the slender-body analysis will be better for dielectric drops, where long thin drops are more easily obtained.

It would seem that the main deficiency of the slender-body model is that it does not accurately represent the physics of the problem when $R(x)$ becomes small. When $R(x)$ becomes of size $O(\epsilon)$ surface tension effects become significant, and also, the $R(x)$ dependence of the electric stress becomes important. We believe that these two effects (the latter via the velocity field induced) are important for the formation and pinching-off of lobes. At present, it is not possible for the slender-body equations to result in a drop that pinches off. From (4.35) it can be seen that if $R(x)$ (and thus $W(x)$) approaches 0 at some point $x = a \neq 0$ then

$$\frac{\partial W(a,t)}{\partial t} \approx \tfrac{1}{2}\beta a^2 > 0, \tag{4.45}$$

which prevents the drop from pinching off. The only place a drop can pinch off is at $x = 0$, and even this only occurs as $\ell \to \infty$.

5. Summary and concluding remarks

We have considered the slow deformation of a relatively inviscid conducting drop surrounded by a viscous fluid subject to a uniform electric field. The electric field stretches the drop in the direction of the field. As the drop elongates, surface tension becomes less important except at the drop ends, with the primary balance between viscous and electric stresses.

We first presented some numerical results based on a boundary integral formulation. For weak electric fields we recovered the known equilibrium drop shapes, while for β exceeding some critical value, β_{crit}, we obtained the time evolution of the drops. For electric fields above the critical strength, two charged lobes form and break off from the ends of the drop. The droplets formed are highly charged and are themselves unstable. As the electric field strength increases, the volume of the lobes decreases and eventually the lobe formation disappears – the drop breakup then consists of a highly charged jet-like structure being ejected from the end of the drop. It was seen that for all the drops, the shape was close to spheroidal for aspect ratios up to about 5. Also for electric fields slightly exceeding this critical value, we found that there is a period of slow deformation whose duration grows as β_{crit} is approached from above.

Physically this period of slow deformation for β near β_{crit} has interesting ramifications. For the pedestal insulator problem discussed in the introduction, even after a leak has been fixed, sufficient rainwater might have already leaked inside so that the value of β for the system is above the critical value. In this case breakdown will still occur, though it could take anywhere from 5 days to 5 months for the drop to pass through this region of slow elongation and for any signs of breakdown of the insulator to be seen. (This is based on a value of $\beta = 0.21$. The large variation in time is primarily due to the variation of the viscosity of bitumen with temperature. The period of 5 days corresponds to a temperature of 20 °C, and 5 months corresponds to a temperature of 5 °C.) For industrial processes, such as the purification of liquids using electric fields, this period of slow elongation permits the use of supercritical electric fields for a limited time. This leads to the possibility of using higher pulsed electric fields, instead of weaker continuous electric fields. The asymptotic behaviour close to critical is examined in detail in Dubash & Mestel (2006).

We have also derived equation (4.35), which models the deformation of a slender drop. The model has a similarity solution (albeit unstable) where the shape of the drop is always spheroidal, and where the drop length scales as $(t_c - t)^{-1/3}$. As well, we are able to obtain the general solution for the slender-body equations. Depending upon the initial drop shape we can obtain two different types of drop behaviour. Either there is a finite-time blowup ($\ell \to \infty$ as $t \to t_c$), or a pointed end forms at some finite value of ℓ. In the former case the drop length scales as $(t_c - t)^{-1/3}$ or as $(t_c - t)^{-1/2}$, depending on the structure of $f(x)$ in (4.41). Unfortunately, the slender-body model does not appear to capture properly the dynamics of breakup. Naturally, the slender-body analysis applies best to drops which extend indefinitely, rather than to the observed lobe formation. It turns out that the negligible drop viscosity is responsible for the differences with the breakup mechanism of Sherwood (1988) (i.e. pointed ends). If the drop is given an appreciable viscosity, the formation of lobes disappears and pointed ends can be obtained. How the viscosity of the drop affects the breakup behaviour is presented elsewhere (Dubash & Mestel 2007).

Our formulation assumed that the deformation of the drop was a slow process, i.e. that the Reynolds number of the flow is small. The velocities were highest during the later stages of the deformation, near breakup. If, for example, we take the pedestal insulator problem, where we have a drop of rainwater in bitumen, then $Re \sim 10^{-5}$ near break up, ($\hat{\rho} \sim 10^3\,\mathrm{kg\,m^{-3}}$, $\hat{U} \sim 10^{-4}\,\mathrm{m\,s^{-1}}$, $\hat{L} \sim 10^{-1}\,\mathrm{m}$, $\hat{\mu} \sim 10^3\,\mathrm{Pa\,s}$, and $\beta \sim O(1)$). However, if we have a water drop in oil ($\hat{\mu} \sim 1\,\mathrm{Pa\,s}$, $\hat{U} \sim 10^{-1}\,\mathrm{m\,s^{-1}}$), then $Re \sim 10$ near break up. At this point inertial effects could become important, but this is beyond the scope of this work.

N. D. would like to gratefully acknowledge financial support from the Natural Sciences and Engineering Research Council of Canada.

Appendix. Spheroidal approximation model

The spheroidal approximation has been used by Garton & Krasucki (1964), Taylor (1964), and Sherwood (1988) to calculate the equilibrium shapes of conducting drops in an electric field. Taylor (1964) showed that the equilibrium shapes are very close to being spheroidal, thus it is reasonable to assume that shape of the drop as it evolves to equilibrium is also close to spheroidal. Hence, we consider a spheroidal approximation model for the time-dependent deformation of the drop.

We use the prolate spheroidal coordinate system for the mathematical formulation. A more detailed description of the coordinate system can be found in many books; see for example Morse & Feshbach (1953) and Happel & Brenner (1965). The problem is non-dimensionalized using (3.1) and (3.2).

In this work, we use the following construction of the prolate spheroidal coordinate system: $\{(\lambda, \zeta, \phi) : 1 \leqslant \lambda < \infty, -1 \leqslant \zeta \leqslant 1, 0 \leqslant \phi < 2\pi\}$, where

$$x = c\lambda\zeta, \qquad r = c\sqrt{(\lambda^2 - 1)(1 - \zeta^2)}, \tag{A 1}$$

and where x is the distance along the axis of symmetry of the projection of a point onto the axis of symmetry, r is the perpendicular distance of a point from the axis of symmetry, and $x = \pm c$ are the locations of the foci along the axis of symmetry. The coordinate grid is constructed from confocal spheroids ($\lambda =$ constant) and hyperboloids ($\zeta =$ constant). For the spheroid $\lambda = \lambda_0$ the aspect ratio, α is given by

$$\alpha = \frac{\lambda_0}{\sqrt{\lambda_0{}^2 - 1}}. \tag{A 2}$$

We are assuming that the drop deforms smoothly from one spheroid to another, thus we can represent the surface of the drop by $\lambda = \lambda_0(t)$. It should be noted that to conserve mass we require $c = c(\lambda_0(t))$, and thus we have a coordinate system that is moving in time.

For the spheroidal approximation the normal stress condition, (3.4), must be modified. Because we have restricted the shape of the drop to be a spheroid, we cannot, in general, satisfy the stress balance at every point on the surface of the drop. We instead choose to impose the normal stress balance in an average sense through a balance of energy (Taylor 1964; Garton & Krasucki 1964; Sherwood 1988).

Instead of balancing pressures and deviatoric stress with the electric stress and the surface tension, we balance the viscous dissipation with the rates of change of electric field energy and surface tension energy of the drop:

$$\int_\Omega \dot{\boldsymbol{\gamma}}^2 \, \mathrm{d}v + \beta \frac{\mathrm{d}U_e}{\mathrm{d}t} + \frac{\mathrm{d}U_s}{\mathrm{d}t} = 0, \tag{A 3}$$

where $\dot{\boldsymbol{\gamma}} = \sqrt{\dot{\gamma}_{ij}\dot{\gamma}_{ij}/2}$ is the second invariant of the rate-of-strain tensor, U_e is the electric field energy, U_s is the surface tension energy of the drop, and β is the dimensionless electric field strength given by (3.3). Equation (A 3) is also equivalent to taking the product of (3.4) with the normal velocity and integrating over the drop surface.

The general solution of (2.2) in spheroidal coordinates is well known (see for example Lamb 1932, Art. 103). Applying boundary conditions (2.3) and (2.4) (along with the condition that $\theta(\lambda, \zeta)$ is finite at $\zeta = \pm 1$) we obtain the electric potential for the field surrounding the drop $\lambda = \lambda_0$:

$$\theta(\lambda, \zeta) = -c\zeta \left[\lambda - \frac{\lambda_0}{Q_1(\lambda_0)} Q_1(\lambda)\right], \tag{A 4}$$

where

$$Q_1(\lambda) = \frac{1}{2}\lambda \ln\left(\frac{\lambda+1}{\lambda-1}\right) - 1, \tag{A 5}$$

is a Legendre function of the second kind.

The general solution of (2.5) in spheroidal coordinates is known (see for example Sampson 1891). Applying the boundary condition at infinity and requiring that ψ is regular at $\zeta = \pm 1$, the general solution reduces to

$$\psi(\lambda, \zeta) = c^2(\lambda^2-1)(1-\zeta^2)\sum_{n=0}^{\infty}[a_n Q_n'(\lambda)P_n'(\zeta) + b_n(Q_{n+2}'(\lambda)P_n'(\zeta) + Q_n'(\lambda)P_{n+2}'(\zeta))], \tag{A 6}$$

where $P_n(x)$ and $Q_n(x)$ are Legendre functions of the first and second kind respectively. We are left with two sets of unknown coefficients, a_n and b_n, to determine.

For computations we truncate (A 6), taking the first $2N$ terms. Applying boundary conditions (2.6) and (2.9) this leads to a finite set of linear equations for the coefficients $b_0, a_2, \ldots, a_{2N}, b_{2N}$, which can be solved. (Note that a_0 is arbitrary as $P_0'(x) = 0$, and is only included for a neat presentation of (A 6), and the odd numbered coefficients are zero due to the symmetry of the problem.)

In spheroidal coordinates the non-dimensional surface tension energy is (O'Konski & Thacher 1953)

$$U_s = 2\pi c^2\left[\left(\lambda_0^2 - 1\right) + \lambda_0^2\sqrt{\lambda_0^2 - 1}\arcsin\left(\frac{1}{\lambda_0}\right)\right]. \tag{A 7}$$

Recalling that both c and λ_0 are functions of time, it can be seen that the rate of change of surface tension energy has the form

$$\frac{\mathrm{d}U_s}{\mathrm{d}t} = f_s(\lambda_0)\frac{\mathrm{d}\lambda_0(t)}{\mathrm{d}t}, \tag{A 8}$$

where $f_s(\lambda_0)$ is only a function of λ_0.

The electric field energy of a conductor in an otherwise uniform electric field is unfortunately infinite. However, we are able to calculate the change in the electric field energy of a uniform field after introducing a conductor into the field. If U_0 is the energy of the initial uniform electric field, and U_e is the energy of the uniform field with the conductor present, then from Stratton (1941)

$$U_0 - U_e = \frac{1}{2}\int_{\Omega_d}\mathrm{d}v + \frac{1}{2}\int_{\Omega}((0,0,1) - \boldsymbol{E})^2\,\mathrm{d}v, \tag{A 9}$$

where $\boldsymbol{E} = -\nabla\theta$ is the electric field with the conductor present. So the rate of change of electric field energy also has the form

$$\frac{\mathrm{d}U_e}{\mathrm{d}t} = -\frac{\mathrm{d}}{\mathrm{d}t}(U_0 - U_e) = f_e(\lambda_0)\frac{\mathrm{d}\lambda_0(t)}{\mathrm{d}t}, \tag{A 10}$$

where f_e is strictly a function of λ_0.

Finally, to calculate the viscous dissipation we use the result that

$$\frac{1}{2}\int_{\Omega}\tau_{ij}\dot{\gamma}_{ij}\,\mathrm{d}v = \int_{\partial\Omega_d}(-p\delta_{ij} + \tau_{ij})u_i n_j\,\mathrm{d}s, \tag{A 11}$$

where n_j is the outward normal of Ω, i.e. n_j points into the drop. Owing to the axisymmetry, the right-hand side of (A 11) can be reduced to a line integral over the profile of the drop. It turns out that $(\mathrm{d}\lambda_0/\mathrm{d}t)^2$ is a factor of the viscous dissipation.

Taking this into consideration, along with the structure of (A 8) and (A 10), the energy equation, (A 3), can be written as a first-order differential equation for the evolution of λ_0,

$$\frac{\mathrm{d}\lambda_0}{\mathrm{d}t} = -\frac{\beta f_e(\lambda_0) + f_s(\lambda_0)}{f_{\dot{\gamma}}(\lambda_0)}, \tag{A 12}$$

where $f_{\dot{\gamma}}$ is the viscous dissipation with the dependence on the rate of change of λ_0 factored out. For a given initial drop shape, $\lambda_0(0)$, we can solve (A 12) to obtain the evolution of the drop in time. A detailed derivation of the spheroidal model can be found in Dubash (2006).

For all the spheroidal approximation results shown in this paper a fourth-order Runge–Kutta scheme is used to solve (A 12). We have also taken $N = 5$. When N is increased no noticeable change occurs in the evolution of the drop, except at very high aspect ratios for which the entire model is not considered accurate. For the spheroidal approximation model $\beta_{crit} \doteq 0.2044$. For purposes where the details of breakup are unimportant, this spheroidal model provides a fast, accurate alternative to full numerical computations.

REFERENCES

Abbi, S. S. & Chandra, R. 1956 On the equilibrium of a small conducting liquid drop in a uniform external electric field. *Proc. Nat. Sci. India* A **22**, 363–368.

Baygents, J. C., Rivette, N. J. & Stone, H. A. 1998 Electrohydrodynamic deformation and interaction of drop pairs. *J. Fluid Mech.* **368**, 359–375.

Brazier-Smith, P. R. 1971 Stability and shape of isolated and pairs of water drops in an electric field. *Phys. Fluids* **14** (1), 1–6.

Buckmaster, J. D. 1972 Pointed bubbles in slow viscous flow. *J. Fluid Mech.* **55** (3), 385–400.

Buckmaster, J. D. 1973 The bursting of pointed drops in slow viscous flow. *J. Appl. Mech.* **40** (1), 18–24.

Dubash, N. 2006 Behaviour of a conducting drop in a viscous fluid subject to an electric field. PhD thesis, Imperial College London.

Dubash, N. & Mestel, A. J. 2006 Behaviour near critical for a conducting drop in an electric field. *Phys. Fluids* (submitted).

Dubash, N. & Mestel, A. J. 2007 Breakup behavior of a conducting drop suspended in a viscous fluid subject to an electric field. *Phys. Fluids* (in press).

Eow, J. S. & Ghadiri, M. 2003 Motion, deformation and break-up of aqueous drops in oils under high electric field strengths. *Chem. Engng Process.* **42**, 259–272.

Eow, J. S., Ghadiri, M. & Sharif, A. 2001 Deformation and break-up of aqueous drops in dielectric liquids in high electric fields. *J. Electrostat.* **51**, 463–469.

Feng, J. Q. & Scott, T. C. 1996 A computational analysis of electrohydrodynamics of a leaky dielectric drop in an electric field. *J. Fluid Mech.* **311**, 289–326.

Garton, C. G. & Krasucki, Z. 1964 Bubbles in insulating liquids: stability in an electric field. *Proc. R. Soc. Lond.* A **280**, 211–226.

Grigor'ev, A. I., Sharov, A. N. & Shiryaeva, S. O. 1999 Stability of a bubble in a dielectric liquid in an external electrostatic field. *Tech. Phys.* **44** (8), 908–912.

Ha, J.-W. & Yang, S.-M. 2000 Deformation and breakup of Newtonian and non-Newtonian conducting drops in an electric field. *J. Fluid Mech.* **405**, 131–156.

Happel, J. & Brenner, H. 1965 *Low Reynolds Number Hydrodynamics, with Special Applications to Particulate Media*. Prentice Hall.

Hirata, T., Kikuchi, T., Tsukada, T. & Hozawa, M. 2000 Finite element analysis of electrohydrodynamic time-dependent deformation of dielectric drop under uniform DC electric field. *J. Chem. Engng Japan* **33** (1), 160–167.

Lamb, H. 1932 *Hydrodynamics*, 6th edn. Cambridge Univeristy Press.

Li, H., Halsey, T. C. & Lobkovsky, A. 1994 Singular shape of a fluid drop in an electric or magnetic field. *Europhys. Lett.* **27** (8), 575–580.

Mestel, A. J. 2002 Maximal accelerations for charged drops in an electric field. *Phys. Fluids* **14** (4), 1396–1402.

Miksis, M. J. 1981 Shape of a drop in an electric field. *Phys. Fluids* **24** (11), 1967–1972.

Morse, P. M. & Feshbach, H. 1953 *Methods of Theoretical Physics*. McGraw-Hill.

O'Konski, C. T. & Thacher, H. C. 1953 The distortion of aerosol droplets by an electric field. *J. Phys. Chem.* **57**, 955–958.

Pozrikidis, C. 1992 *Boundary Integral and Singularity Methods for Linearized Viscous Flow*, 2nd edn. Cambridge University Press.

Pozrikidis, C. 1997 *Introduction to Theoretical and Computational Fluid Dynamics*. Oxford University Press.

Ramos, A. & Castellanos, A. 1994 Conical points in liquid-liquid interfances subjected to electric fields. *Phys. Lett.* A **184**, 268–272.

Rayleigh, Lord 1882 On the equilibrium of liquid conducting masses charged with electricity. *Philos. Mag.* **14**, 184–186.

Sample, S. B., Raghupathy, B. & Hendricks, C. D. 1970 Quiescent distortion and resonant oscillations of a liquid drop in an electric field. *Intl J. Engng Sci.* **8**, 97–109.

Sampson, R. A. 1891 On Stokes's current function. *Phil. Trans. R. Soc. Lond.* A **182**, 449–518.

Sherwood, J. D. 1988 Breakup of fluid droplets in electric and magnetic fields. *J. Fluid Mech.* **188**, 133–146.

Sherwood, J. D. 1991 The deformation of a fluid drop in a electric field: a slender-body analysis. *J. Phys.* A*: Math. Gen.* **24**, 4047–4053.

Stone, H. A., Lister, J. R. & Brenner, M. P. 1999 Drops with conical ends in electric and magnetic fields. *Proc. R. Soc. Lond.* A **455**, 329–347.

Stratton, J. A. 1941 *Eletromagnetic Theory*. McGraw-Hill.

Taylor, G. I. 1934 The formation of emulsions in definable fields of flow. *Proc. R. Soc. Lond.* A **146**, 501–523.

Taylor, G. I. 1964 Disintegration of water drops in an electric field. *Proc. R. Soc. Lond.* A **280**, 383–397.

Taylor, G. I. 1966*a* The force exerted by an electric field on a long cylindrical conductor. *Proc. R. Soc. Lond.* A **291**, 145–158.

Taylor, G. I. 1966*b* Studies in electrohydrodynamics i. the circulation produced in a drop by electric field. *Proc. R. Soc. Lond.* A **291**, 159–166.

Tillett, J. P. K. 1970 Axial and transverse Stokes flow past slender axisymmetric bodies. *J. Fluid Mech.* **44** (3), 401–417.

Wilson, C. T. R. & Taylor, G. I. 1925 The bursting of soap bubbles in a uniform electric field. *Proc. Camb. Phil. Soc.* **22**, 728–730.